ELSEVIER

Polymer 43 (2002) 6785–6794

polymer

www.elsevier.com/locate/polymer

Nanofiber garlands of polycaprolactone by electrospinning

D.H. Reneker[a,*], W. Kataphinan[a], A. Theron[b], E. Zussman[b], A.L. Yarin[b]

[a]*Maurice Morton Institute of Polymer Science, The University of Akron, 170 University Circle, Akron, OH 44325-3909, USA*
[b]*Faculty of Mechanical Engineering, Technion, Haifa 32000, Israel*

Received 10 June 2002; received in revised form 15 August 2002; accepted 19 August 2002

Abstract

Over a period of time, the typical path of a single jet of polymer solution, in the electrospinning process follows the nearly straight electric field lines for a certain distance away from the tip, and then develops a series of electrically driven bending instabilities that cause the path of the jet to explore a cone shaped envelope as the jet elongates and dries into a nanofiber. The multitudes of open loops that are formed are rarely observed to come into contact with each other until the dry nanofiber is collected at the end of the process.

A new phenomenon is reported in this paper. Electrospinning a solution of polycaprolactone in acetone caused the dramatic appearance of a fluffy, columnar network of fibers that moved slowly in large loops and long curves. The name 'garland' was given to the columnar network.

Open loops of the single jet came into contact just after the onset of the bending instability and then merged into a cross-linked network that created and maintained the garland. Contacts between loops occurred when the plane of some of the leading loops of the jet rotated around a radius of the loop. Then a small following loop, expanding in a different plane, intersected a leading loop that was as many as several turns ahead. Mechanical forces overcame the repulsive forces from the charge carried by the jet, the open loops in flight made contact and merged at the contact point, to form closed loops.

The closed loops constrained the motion to form a fluffy network that stretched and became a long roughly cylindrical column a few millimeters in diameter. This garland, which was electrically charged, developed a path of large open loops that are characteristic of a large-scale electrically driven bending instability. Over a long period of time, the fluffy garland never traveled outside a conical envelope similar to, but larger than the conical envelope associated with the bending instability of a single jet.

Keywords: Electrospinning; Biodegradable nanofibers; Polycaprolactone nanofiber

1. Introduction

Electrospinning of nanofibers and nanotubes allows generation of fibers with diameters in a wide range around 100 nm [1–6]. Much of the nanofiber research reported so far was on nanofibers made from polyethylene oxide (PEO) solutions and mixtures of PEO with other polymers [7,8]. Nanofibers were collected in the form of non-woven mats [1–4], or in the form of oriented arrays or braids [5]. Interest in biomedical applications [9–11], and in applications as sensors [12], is developing rapidly. Methods for coating nanofibers with metals, carbon and semiconductors were reported [13]. Mathematical models [2,4,14–17], which examine the stability of jet paths and of the cone-like surfaces from which the jets emerged, were developed. Bead formation on electrospun jets due to capillary instability driven by surface tension is typically prevented by significant viscoelastic stresses. The electrospun jets bend due to mutual repulsive force between the electric charges transported by the jets [2,4]. The bending instability is not an anomaly, but an essential part of the process that elongated the jet and eventually formed the nanofibers.

Garland formation is a distinct phenomenon associated with electrospinning that results in novel, potentially useful nanofiber structures. In a number of applications, such as textiles [18,19], advanced filter media made of nanofibers [20] or microaerodynamic decelerators based on permeable surfaces of nanofiber mats [21], fluffiness may be beneficial. In the case of microaerodynamic decelerators, nanofibers that are as strong as possible are needed to withstand turbulence. In the present work, garlands of polycaprolactone (PCL) nanofibers were generated and the processes that produce garlands were examined. Garlands of

* Corresponding author. Tel.: +1-330-972-6949; fax: +1-3330-972-5290.
E-mail address: dhr@polymer.uakron.edu (D.H. Reneker).

0032-3861/02/$ - see front matter
PII: S0032-3861(02)00595-5

polycaprolactone were observed for other solvents, for other polymers such as a copolymer of vinylidene fluoride and tetrafluoroethylene, and for polyethyloxazoline dissolved in acetone. The conditions for the formation of garlands were reproducible. Loops, which formed in a different way in a single jet of polyhydroxyethyl methacrylate dissolved in a mixture of ethanol and formic acid, were described by Koombhongse et al. [22]. These loops had a larger scale and did not lead to the observation of garlands.

2. Experiment

Experiments on electrospinning were performed with an apparatus similar to that used in previous work [1–5]. The following polymer solutions were prepared for this study.

Polycaprolactone, acronym PCL, chemical formula $[O(CH_2)_5CO]_n$, with a molecular weight of 80 000 g/mol, was dissolved in acetone at concentrations between 14 and 18%. All the observations are characteristic of a nominal concentration of 15%. The polymer was purchased from Aldrich. A 15% (nominal) solution of PCL with a molecular weight of about 120 000 g/mol was also used.

Some of the solutions were characterized by measuring the electrical conductivity and viscosity. The viscosity was measured at shear rates from 10^{-3} to 10^{+3} s^{-1} using a Rheometrics Dynamic Stress Rheometer. On a log–log plot, the shear viscosity decreased linearly between 10^{-3} and 1 s^{-1}, from 100 to about 5 Pa s, and then remained constant from 1 to 1000 s^{-1}. The electrical conductivity was measured by applying a voltage in the range from 5 to 30 V and measuring the current through a column of fluid in a glass tube with known cross-sectional area and length.

In a typical electrospinning experiment, the polymer solution was held in a syringe or glass pipette with an opening at the tip that had a diameter of a few hundred microns. The solution was delivered to the tip by the hydrostatic pressure of a liquid column a few centimeters high. A wire inserted into the solution was connected to a high-voltage power supply. Frames to collect the electrospun nanofibers, about 10 cm square, and supported on table-like legs, were made of balsa-wood sticks with a diameter of 3 mm. The frames were placed 30 cm below the syringe tip and 5 cm above the ground plane.

Jets issuing from the droplets of PCL solution at the exit of the syringe nozzle were photographed at rates up to 2000 frames/second with exposure times as short as 0.025 ms (Motionscope Redlake Imaging). The jets from the syringe were illuminated by a 400-W Hydrar-gyrum medium arc-length iodine lamp, which is a quasi-continuous light source used in conjunction with an electronic ballast (Dedolight). The jets from the glass pipette were illuminated with a xenon arc lamp in combination with a diffuser and a Fresnel lens [2]. Morphological features of the electrospun fibers were observed with optical microscopes (Zeiss or Wild), with an atomic force microscope, (AFM Nanoscope III, Digital Instruments, Veeco), and with a scanning electron microscope (JEOL).

In another set of experiments, polymer solutions were electrospun from a glass pipette with a tip diameter about 300–400 μm and from a metal cone with a tip diameter about 1.5 mm and a vertex angle of about 25 °. Jets were produced when the electrical potential difference between the tip and the collector was in the range from 5 to 30 kV and the distance between the spinneret and ground was in the range from 7 to 30 cm. The electric field strengths for the experiments described in this paper ranged from 0.18 to 0.54 kV/cm. The fibers were collected on sheets of aluminum foil, on metal screens, and glass microscope slides. The garlands were photographed at a scale of 10 cm and a rate of 30 frames/second with a VHS video camera (Samsung).

3. Observations

3.1. The straight segment of the jet

The diameter of the straight segment of a typical jet was measured by observing the first maxima in the interference pattern created when the jet was illuminated with a 1 mm diameter neon laser beam. The straight segment, which was around 3 mm long, had a diameter between 5 and 10 μm near its midpoint. Increasing the voltage increased the diameter of the jet. The diameter varied with time, and the jet swung in and out of the beam. The video record of the position of the first maximum of the scattered light enabled a measurement to be made at a time when the jet was centered in the laser beam.

3.2. The onset of the bending instability, formation of closed single loops and double loops

Fig. 1 shows 30 successive images of a region that includes most of the straight segment, the onset of the bending instability and the region where single, small closed loops were observed. The onset of the bending instability is shown in the first 12 frames. The exposure time for each frame was 0.025 ms, and the time between frames was 0.5 ms. Various parts of the jet moved downward at slightly different velocities near 1 m/s.

The onset of the bending instability was suppressed, from unknown causes, for about 6 ms, prior to the first frame of this series. The first four frames of Fig. 1 show, in the top half of the frames, the reestablishment of the bending instability, as the loops in the leading part grow to a diameter of 3 mm. The path of the jet is complicated and not clearly observed at every point. In frame 6, a closed single loop about 1 mm in diameter is partly visible as it extended from the lower right part of the developing instability. This small loop, indicated by arrows in frames 6, 12, and 18, was followed until it moved out of the right edge of frame 18.

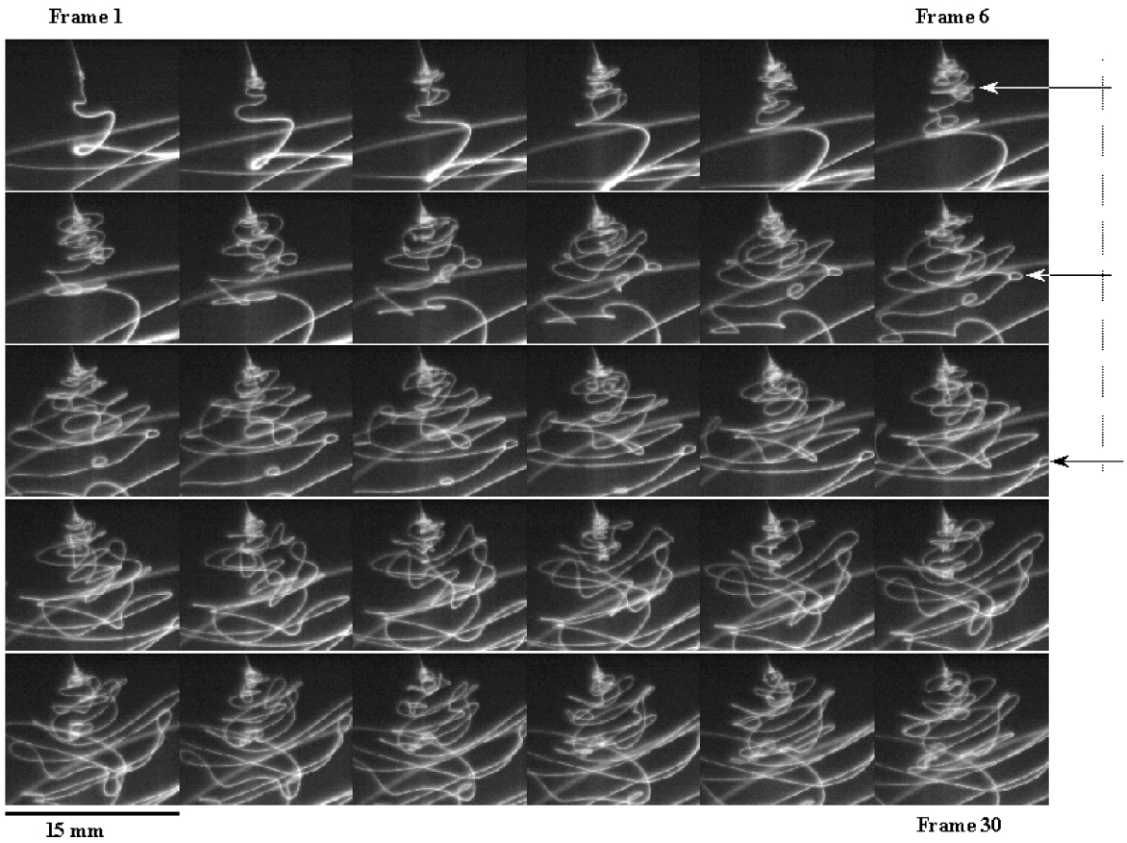

Fig. 1. Frame by frame images that show the evolution of the bending instability on a jet of 15% PCL in acetone. (5 kV, 240 mm gap, 2000 frames/second, 0.025 ms exposure).

By frame 18, (8.5 ms after frame 1), the path reached the dimensions and the level of complexity that was typical of this region. The path of the jet, after the onset of bending, lies within a volume called the envelope cone [2]. The centers of many of the loops were displaced radially from the projected axis of the straight segment. The loops, which extended outward from the axis and reached a diameter of around 15 mm, tilted as the side of the loop closest to the axis of the straight segment moved downward more rapidly than the other side. Segments of these larger loops formed the long tilted lines seen most clearly in the bottom half of frames 25–30. As the perimeter of a small loop near the axis elongated, it contacted the tilted loops that preceded it, thereby providing an opportunity for the fluid segments to merge and form a permanent connection. The connections that form closed loops lead to the formation of garlands, in ways that are described below.

Other observations similar to Fig. 1 were made. The

Table 1
Envelope cone at the first bending instability of a single jet

Potential, distance from tip to collector, and electric field	5 kV, 140 mm, and 0.36 kV/cm	7.5 kV, 140 mm, and 0.54 kV/cm
Advance per loop (mm/loop)	1.4	Not observable
Downward velocity (m/s)	0.7 ± 0.2	1.8 ± 0.5
Length of straight segment (mm)	3	>3
Vertex angle of envelope cone	95°	Not observable

Table 2
Experimental and electrical parameters

Solution	Electrical parameters				
	Potential (kV)	Gap (mm)	Current (nA)	Conductivity (μS/cm)	Flow rate (mg/s)
15% PCL in acetone	7.5	140	105 ± 15	4.7 ± 0.6	25 ± 2
	5		35 ± 15		9 ± 2

Table 3
Envelope cone of the bending instability of curly garlands

Potential and distance from tip to collector	5 kV and 140 mm	7.5 kV and 140 mm
Advance per loop (mm/loop)	10	20
Cross-sectional diameter of the garland (mm)	4 ± 1	6 ± 1
Vertex angle of garland envelope cone (°)	35 ± 3	33 ± 3

Table 3 summarizes observations of the paths of garlands after the bending instability occurred.

same solution was spun from the same experimental arrangement and the behavior of the jet and of the garland was observed at potentials of 5 and 7.5 kV. Observations are summarized in Tables 1, 2, and 3.

Double loops were also found. The bending instability generated a somewhat irregular spiral, which, as seen in Fig. 2, soon developed contacts between the turns of the spiral. The contacts persisted. Large irregular loops and small ring-like loops were formed. A small double loop is indicated by a white arrow, and magnified in the inset in the frame shown at the lower left corner.

The loops of the jet observed at 5 kV progressed downward at a rate near 0.7 m/s. The outer parts of the largest open loops were often involved in the formation of closed loops. In Fig. 2, there were about seven complete loops of the path of the jet per centimeter along the axis, so the average advance per loop was 1.4 mm. Identifying loops was difficult, and the advance per loop increased with distance from the tip, so this is only a representative number. The bending instability developed inside an envelope cone that had a total angle at the vertex of about 95°. Information about the advance per loop and vertex angle of the envelope cone for a single jet is summarized in Table 1.

The merged contacts cannot be identified in a single frame of the video sequence, because most of the crossing points seen are projections of the jet path into a plane, and do not represent actual contacts in three-dimensional space. The persistence of a crossing point in many successive frames is a necessary but not sufficient criterion for a permanent attachment. Mechanical contacts where segments of solid fibers crossed, and bent over each other, with no evidence for permanent merging, were also observed.

3.3. Formation of merged contacts

The merged contacts were established when the momentum of the segments and the tension in the jet forced a fluid segment to contact another segment, in spite of the repulsive Coulomb forces. Upon contact, surface tension immediately tended to hold the jets together, while charge tended to flow away from the point of contact. Since the electric charge moved almost with the motion of the liquid [2,4], the large elongation of the jet segments led to a dramatic decrease in the charge per unit length of the jet. Segments separated by relatively large distances along the path of the jet contacted each other during the complicated motions associated with the bending. The two liquid sections in contact merged, due to the effect of surface tension, if the reduction of the surface energy due to merging was greater than the local increase of the energy of the electric field. This yields the following

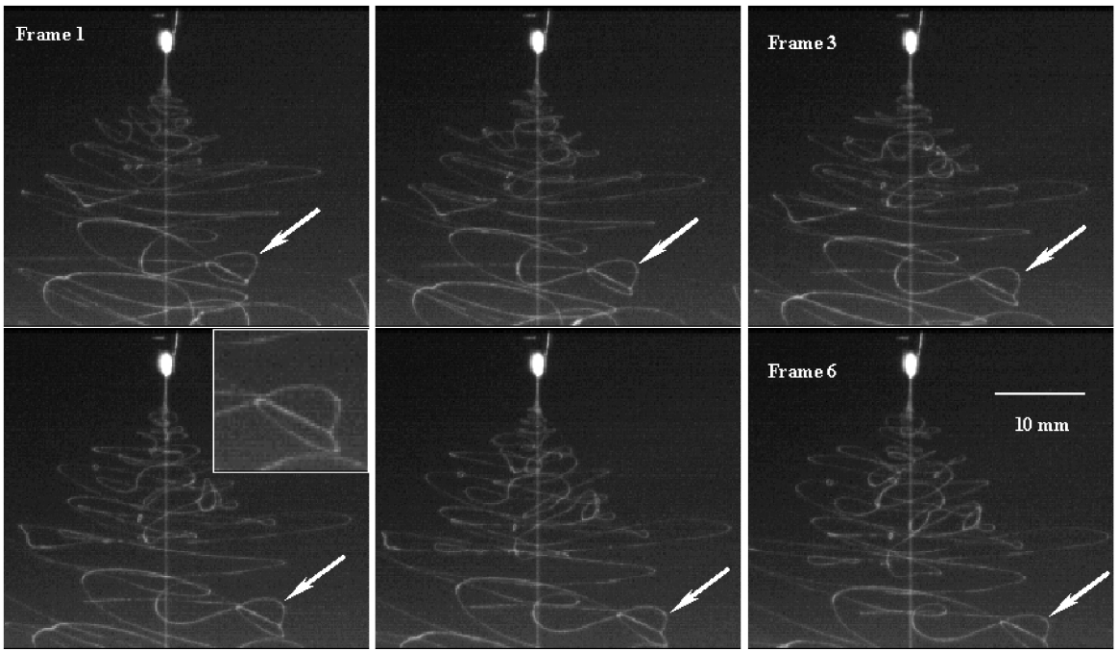

Fig. 2. Small, sometimes complicated, loops that formed immediately after the onset of the bending instability on jets of 15% PCL. The arrow marks a double loop. The vertical line is caused by light scattered from the tip. (5 kV, 140 mm, 500 frames/second, 0.2 ms exposure).

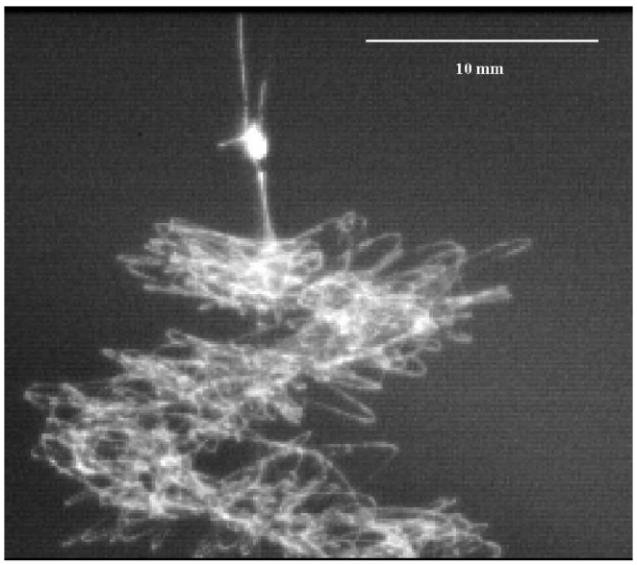

Fig. 3. This image of a jet of a 15% PCL solution shows the onset of the electrically driven bending instability in the garland. (7.5 kV, 140 mm, 1000 frames/second, 0.1 ms exposure).

condition for permanent merging

$$\frac{32\pi^2\varepsilon_0 d\sigma}{E^2} > 1 \qquad (1)$$

Here d is the cross-sectional jet diameter in meters; $\varepsilon_0 = 8.85 \times 10^{-12}$, the permittivity of free space in units of $C^2/N\,m^2$; E, the charge per unit length on the jet in units of C/m and σ is the surface tension in units of N/m. The CGS units customarily used in fluid mechanics can be used in the same equation if ε_0 is set equal to one. If this inequality is fulfilled, two segments of the fluid jet, which have come into contact, can lower their energy if they merge. In our experiments, the jet current at 5 kV was about 35 nA, and at 7.5 kV, about 105 nA (Table 2). At a position below the onset of the bending instability the jet moved downward at a velocity of 0.7 ± 0.2 m/s for 5 kV and at 1.8 ± 0.5 m/s for 7.5 kV. The charge per unit length, E, for 5 kV was 50 ± 35 nC/m, and for 7.5 kV, 58 ± 25 nC/m. The cross-sectional diameter was about 7 ± 2 μm for 5 kV, and 13 ± 4 μm for 7.5 kV. The surface tension of acetone is 0.023 N/m, which yields for the left-hand side of the inequality (1) a value of 2.9 for $d = 9$ μm, $E = 15$ nC/m and 5 kV, and a value of one for $d = 13$ μm, $E = 33.3$ nC/m and 7.5 kV. Both values are of the order of one. Given the fact that Eq. (1) is an order of magnitude estimate, the values of the left-hand side obtained allow the possibility of merging, at least at certain values of the parameters.

Systematic errors were also present. The contact and merging occurred somewhat below the onset of the bending instability. The diameter was measured near the center of the straight segment, somewhat above the location of the bending instability. It was necessary to extrapolate the change in the diameter that occurs as the jet travels from the place where it was measured to the place where contact and merging were observed.

The charge per unit length was determined from the ratio of current to downward velocity. The downward velocity was measured a little below the region where contact and merging occurred, and the velocity increased with distance from the tip (Fig. 4). The variation of the current with time was another major source of this uncertainty.

The uncertainty from systematic errors could be as large as 150%. Removal of systematic errors in diameter and charge per unit length would result in a lower value for the left hand side of the inequality. The data in this paper provide only a broad test of the inequality. In future experiments, the inequality can be tested more precisely if the above data are measured at the place where the contact and merging are observed to occur, and all the measurements are made at the same instant.

Merging converted the jet path between segments into a closed loop (see Figs. 1 and 2, for example). The segments

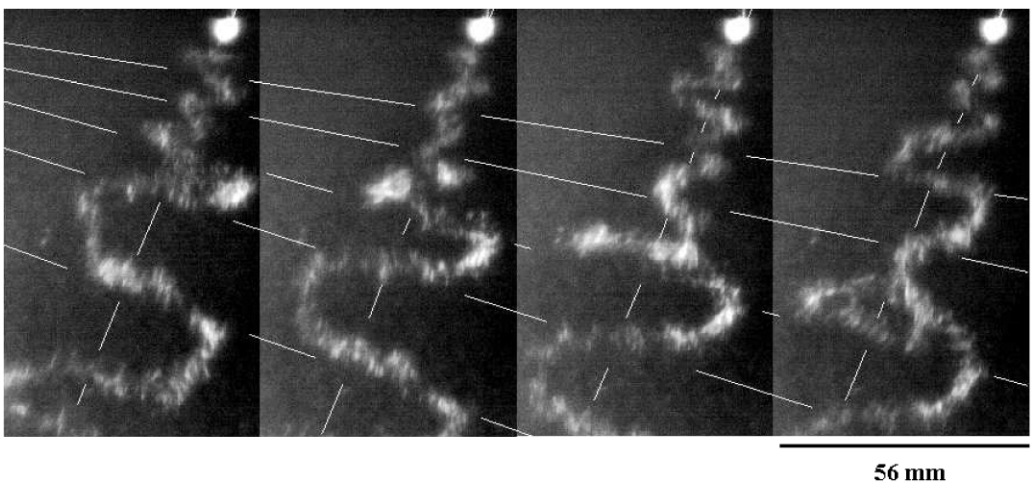

Fig. 4. Motion of a curly garland from a 15% PCL solution is shown. The white lines demarcate segments of a garland that advanced downward. The slope of the top line corresponds to 0.58 m/s, and the slope of the lower lines, successively, to 0.7, 1.05, 1.36, and 2.04 m/s. Since only every fifth frame is shown, the time separation between the frames shown was about 20 ms. (7.5 kV, 140 mm gap, 250 frames/second, 2 ms exposure time).

in the small loop continued to elongate. In Fig. 2 the projection of the loop diameter into the image plane of the loops shown in the inset grew by 17 ± 3% while the projection of large nearby loops grew by 24 ± 4%.

This contacting and merging together of the fluid jet segments created a three-dimensional garland with many closed loops of various sizes. Observations of the structure of the garland discussed below provide additional evidence that supports crossing and permanent merging of fluid loops as an important part of the mechanism for garland formation.

3.4. The bending instability of the garland

The internal structure of the garland varied in different experiments, and this difference between experiments affected some of the observed features of the garland.

When the applied potential was 7.5 kV, and the distance from tip to collector was 14 cm, a garland was created that had a cross-sectional diameter of about 5 ± 1 mm.

The garland followed a large scale looping and spiraling path, similar in shape to that produced by the electrically driven bending instability in a single jet. Electrically driven bending instability of the garland occurred as the garland emerged from the region a few millimeters below the tip, where the merging of segments from different loops occurred (Fig. 3). The advance along the axis per loop of the garland was about 2 cm. Both the diameter of the garland loops and the advance per loop of the garland grew larger as the loops moved downward (Fig. 4). Elongation of the individual fibers and the straightening of the closed loops both contributed to the elongation of the garland. The path of the garland changed with time, but remained inside an envelope cone that had a total angle at the vertex of 33 ± 3° (Fig. 4). The diameter of the loops of the garland did not increase uniformly. Loops with larger and smaller diameters followed each other in ways that allowed the centers of the large loops to be offset radially from the axis. This offset arrangement reduced the number of large loops and generated an envelope cone that had a large vertex angle without requiring a large elongation of the path of the garland.

The electrical forces between the segments of the garland which were separated by distances much large than the diameter of the garland can be usefully approximated by a series of pointlike charges spaced along the flexible garland, just as was done for a single flexible jet in Ref. [2]. The complicated small-scale internal structure within a garland segment, and the corresponding complicated charge distribution of charge within the garland can be averaged to a single quantity of charge at the centroid of the segment. According to Ref. [2], such a system of charges is subject to a bending instability that can produce garland paths of the sort shown in Figs. 3 and 4.

Other observations of the development of an envelope cone of a garland are shown in the superimposed video and flash pictures in Fig. 5(a) and (b). These images were made with an unsynchronized flash lamp, which produced a 0.2 ms long flash, at a repetition frequency lower than the frame rate of an ordinary video camera. The instantaneous path of the garland was recorded whenever the brief flash occurred in the midst of the 16.7 ms exposure of a video frame. The video camera also recorded the average intensity of light scattered from the many other loops that passed through the envelope cone during the 16.7 ms exposure time. The integrated light scattered from all these loops produced the bright area near the onset of the bending instability, and a perceptible gray background in the lower part of the

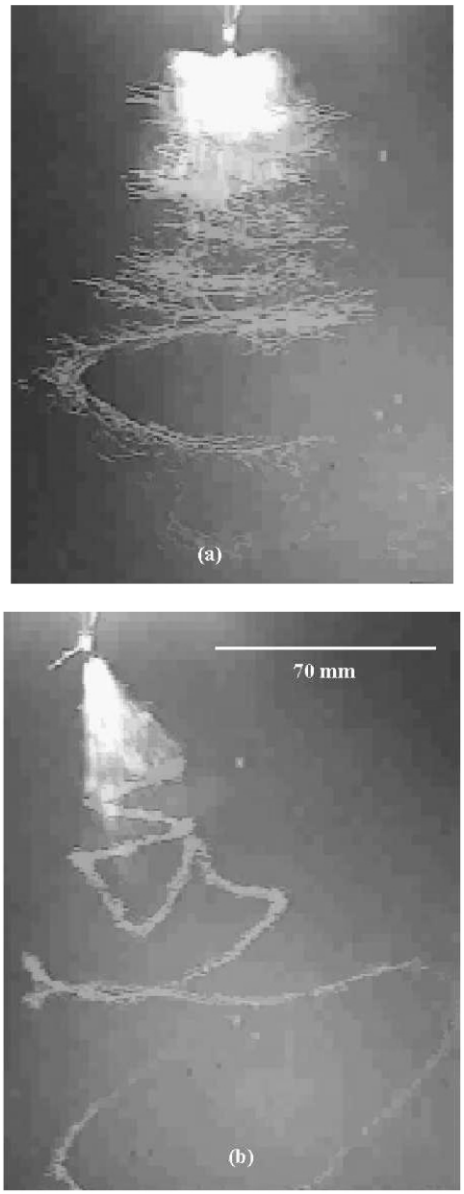

Fig. 5. (a) Segments of individual nanofibers are visible along the bending path of the garland. This was a relatively high flow rate jet from a conical metal tip with a larger opening. (b) Lower flow rate (23.7 kV, 320 mm gap, 30 frames/second, 16.7 ms exposure time). Duration of the xenon strobe light was 0.2 ms.

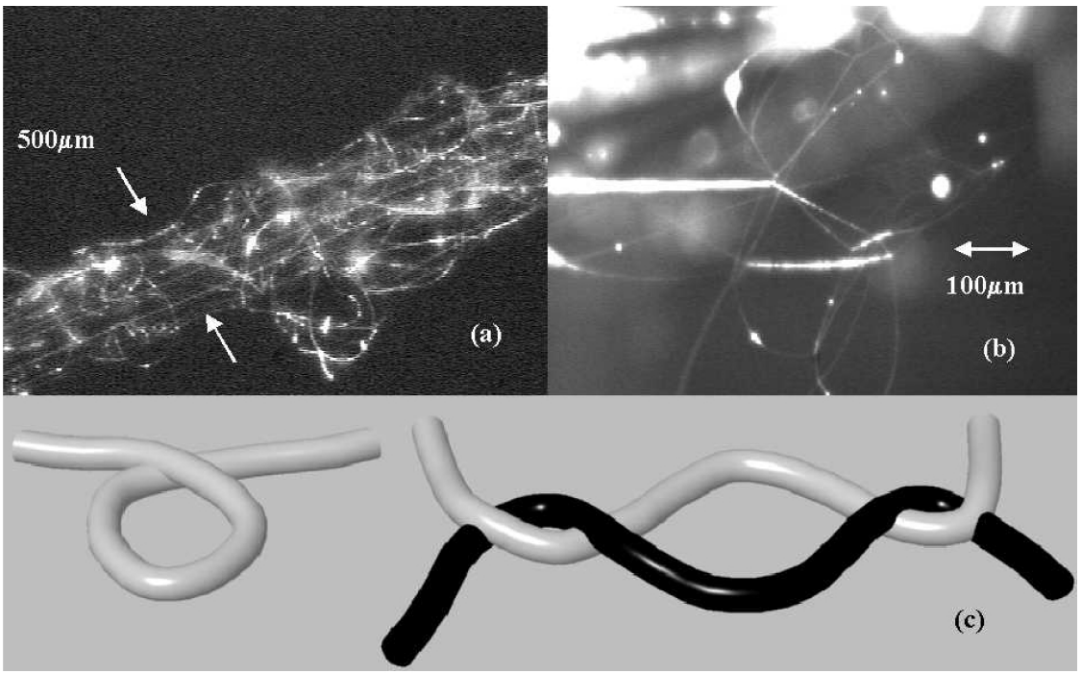

Fig. 6. (a) Optical image of curled and self-entangled nanofiber garland, made from a 14% PCL in acetone, and collected on a balsa-wood frame. (b) Higher magnification view of the garland, showing the nanofiber entangled with itself. The diagrams in (c) show single and double loops that are topologically similar to those observed in Figs. 1 and 2.

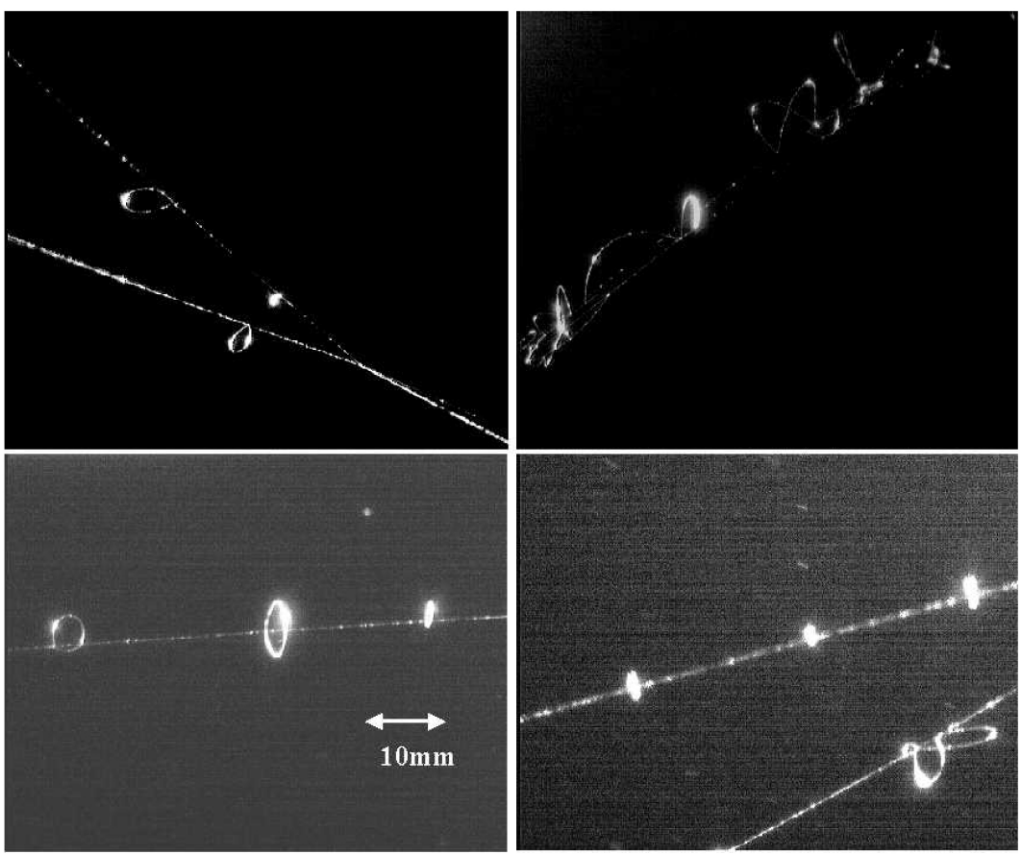

Fig. 7. Optical images of single loops on long nanofibers that were collected on a balsa-wood frame. Single, double and more complicated kinds of loops are shown.

figures. Intervening frames, not shown, during which no flash occurred, recorded only this integrated light. The events in the bright area just below the tip of the pipette lead to the formation of the garland. Detailed examples of the instantaneous jet path in this bright area are shown in Figs. 1–3.

Fig. 5(a) shows a larger scale garland a few centimeters across, that formed loops with diameters of 10 or 15 cm. The higher flow rate in Fig. 5(a) produced unusually large loops which were inclined, and filled a 'square shouldered' envelope region just below the onset of the envelope cone, which is barely visible in this figure. Fig. 3 is an instantaneous image of a jet path that contributed to the time averaged image of Fig. 5(a). The lower flow rate shown in Fig. 5(b) produced loops that stayed within the more usual conical envelope. The maximum radial excursions of the paths, revealed by a brief flash, defined similar cones in the lower parts of Fig. 5(a) and (b).

4. Structure observed in collected, dry garlands of polycaprolactone

Segments of the garlands were collected on glass microscope slides, on balsa-wood frames, and on wire grids with holes about 1 or 2 cm across (Fig. 6). The fibers were mechanically joined at many points. Many of the loops had one or more segments stretched into straight lines and other segments that were curved. Some loops consisted of one elastically bent, semicircular fiber joined at two places to a stretched fiber. Diagrams of single and double loops are shown in Fig. 6(c). Many single loops were found. Double loops and more complicated entanglements were also present.

The long straight fibers in Fig. 7 were pulled tight as they became attached to the frame. Single, double and more complicated loops were observed on the straight fibers. The creation of these loops was not followed in detail.

A garland, captured by sweeping a glass slide through the region just below the onset of the bending instability, was examined with a polarizing microscope. The thicker fluid segments, with diameters of several microns, solidified by nucleation and growth of small spherulites. The surface of these thicker fibers showed rough spots. At low magnification, both the spherulites and the rough surfaces appeared as bright spots similar to those in the long fibers of Fig. 7. The thinner fibers in a garland were uniformly birefringent, indicating good alignment of the molecular axes with the fiber axis, and showing no evidence of spherulites.

The crystallization behavior of the fibers showed that some of the crossed fibers came into contact before one or both of the fibers were solidified. Consider the case of an uncrystallized fluid jet that came into contact with a small, highly aligned and crystallized fiber. The chains in the small fiber provided an oriented nucleus that caused the chains near the contact point in the fluid segment to begin to crystallize with the same orientation as the chains in the small fiber. The crystallization proceeded in both directions away from the small fiber, before the front of these growing crystals encountered other crystals that were nucleated with other orientations. Fig. 8(a) and (b) show such a region as seen between crossed polarizers. When the thin fiber was at the extinction angle in a polarized light microscope, a dark region was seen in the larger, spherulitic fiber. When the thin fiber was bright, the dark region of the larger fibers was also bright, showing that the small fiber nucleated crystals in which the chains were aligned with the small fiber, rather than forming the small, randomly oriented spherulites that are present in other parts of the larger fiber.

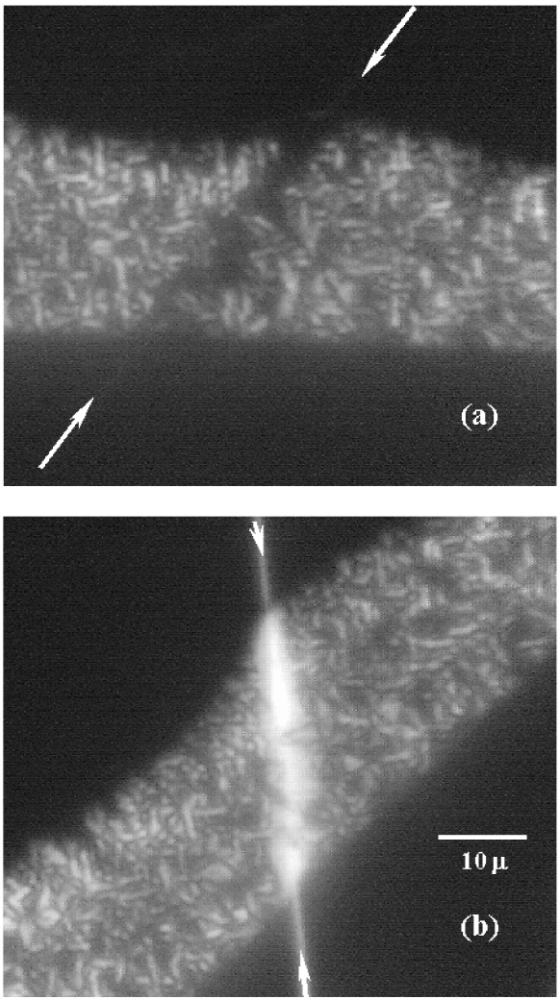

Fig. 8. Polarized light microscope images showing nucleation of crystallites in a fluid jet captured on top of a small, uniformly birefringent fiber of PCL. In (a) the small fiber is aligned in the extinction direction relative to the crossed polarizers, and in (b) the small fiber was rotated to a bright position.

Examples of such merged contacts were found among the fibers in a typical garland collected on a microscope slide. Such oriented regions were too small to produce optical micrographs suitable for publication, but easy to find and to distinguish from unmerged contacts during observation with a high magnification polarizing

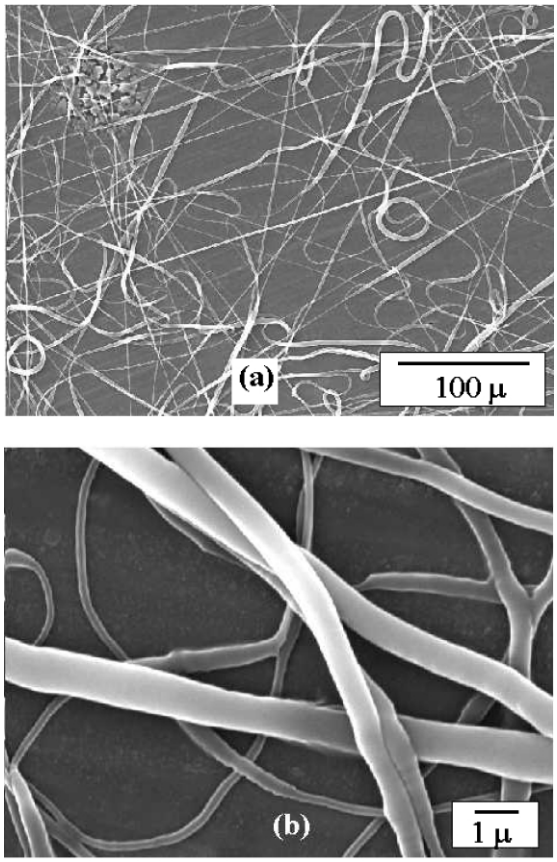

Fig. 9. Scanning electron microscopy images of PCL electrospun fibers collected from the region just below the onset of the bending instability. (a) Wide area showing fibers with large and small diameters, with loops of thick fibers. One fiber that entered the picture near the upper right corner is wavy, indicating the probable occurrence of an electrically driven bending instability. The region from which the fiber was collected was not well localized, since the collector swept across the entire envelope cone, but some of the larger diameter fibers, containing both open and closed loops, were collected from the region near the straight segment. (b) Shows a scanning electron micrograph of the fibers, with both side by side and crossing attachments of fibers. The side-by-side contacts tend to grow longer since the surface energy of the merged fibers is reduced as such contacts elongate.

microscope. Fiber contacts that were not merged occurred after the jet had solidified, probably during collection on the glass slide, and showed no influence of the orientation of the crystals in one fiber by the orientation of the crystals in the other. Not all the merged fibers on the slide were joined in flight, because the collection method, in which a microscope slide was swept though the envelope cone just below the tip, forced many of the fluid jet segments and solid fiber segments to come into contact as they were collected on the slide. The scanning electron micrographs of such a sample, in Fig. 9, showed many contacts of large, probably fluid, fibers and thin, probably crystallized fibers.

In Fig. 10, measurements of the cross-section of three aligned fibers are shown. The data were obtained using an AFM. The fibers had cross-sectional diameters of 1–1.5 μm. Alignment was achieved using the method proposed for generation of oriented arrays and braids [5]. The diameter of the fibers was uniform over each of the 30-μm long segments shown.

5. Summary and conclusions

It was shown that the electrically driven bending instability in the electrospinning of polycaprolactone results in the contact and merging of segments in different loops of the electrospinning jet while the jet was in flight. These contacts limited the lateral expansion of the jet path. A garland, in the form of a long, slender, slow moving and irregular network of electrically charged nanofibers, which had a fuzzy appearance and followed a curly path was created. The curly path of the garland appears to be the result of an electrically driven bending instability that is similar, in many ways, to the bending instability that occurs in a single electrospinning jet.

Polycaprolactone is an interesting candidate for further study of the effects of temperature, elongation, and solvent concentration on the development of morphological structures [23–27] during electrospinning. In particular, the

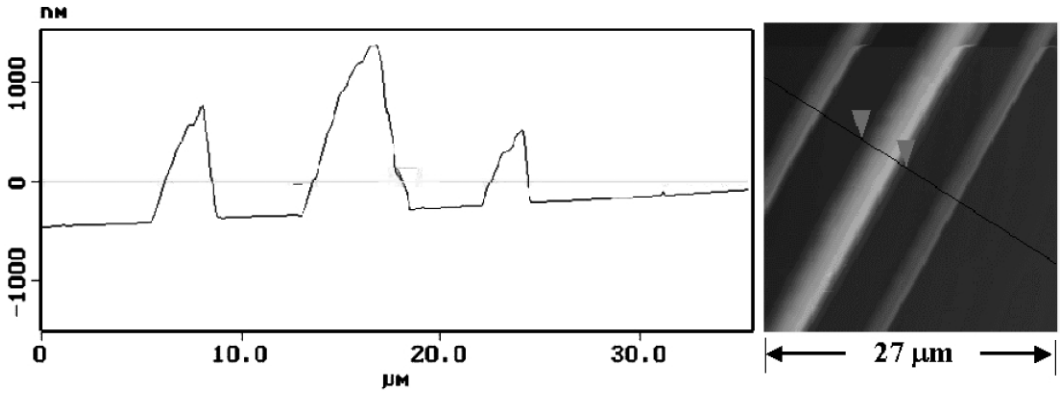

Fig. 10. Diameters of three nanofibers measured by atomic force microscopy. The diameter was measured from the baseline to the maximum height of the peak to eliminate errors from the shape of the tip. The fibers are from 18% PCL in acetone.

nucleation of crystal growth by small, highly oriented fibers of the same polymer can be observed.

Acknowledgements

This research was partially supported by the Israel Science Foundation, and The Israel Academy of Sciences, Grant 287/00-1. The US National Science Foundation grants DMI9813089 and CTS-9900949 also provided support. The high-speed camera was purchased with help from the Hayes Investment Fund of the Ohio Board of Regents.

References

[1] Reneker DH, Chun I. Nanotechnology 1996;7:216–23.
[2] Reneker DH, Yarin AL, Fong H, Koombhongse S. J Appl Phys 2000; 87:4531–47.
[3] Fong H, Reneker DH. In: Salem DR, Sussman MV, editors. Structure formation in polymer fibers. Munich: Hanser; 2000. p. 225–46.
[4] Yarin AL, Koombhongse S, Reneker DH. J Appl Phys 2001;89: 3018–26.
[5] Theron A, Zussman E, Yarin AL. Nanotechnology 2001;12:384–90.
[6] Bognitzki M, Czado W, Frese T, Schaper A, Hellasig M, Steinhart M, Greiner A, Wendorff JH. Adv Mater 2001;13:70–2.
[7] Jaeger R, Schonherr H, Vancso GJ. Macromolecules 1996;29: 7634–6.
[8] Deitzel JM, Kleinmeyer JD, Hirvonen JK, Beck Tan NC. Polymer 2001;42(19):8163–70.
[9] Li W, Laurencin CT, Caterson EJ, Tuan RS, Ko FK. J Biomed Mater Res 2002;60(4):613–21.
[10] Buchko CJ, Kozloff KM, Martin DC. Biomaterials 2001;22: 1289–300.
[11] Boland ED, Bowlin GL, Simpson DG, Wnek GE. Polym Mater Sci Engng 2001;85:51–2.
[12] Zhang Y, Dong H, Norris ID, MacDiarmid AG, Jones WE. Polym Mater Sci Engng 2001;85:622–3.
[13] Bognitzki M, Hou H, Ishaque M, Frese T, Hellwig M, Schwarte C, Schaper A, Wendorff JH, Greiner A. Adv Mater 2000;12(9):637–40.
[14] Hohman MM, Shin M, Rutledge G, Brenner MP. Phys Fluids 2001; 13:2201–20.
[15] Hohman MM, Shin M, Rutledge G, Brenner MP. Phys Fluids 2001; 13:2221–36.
[16] Spivak AF, Dzenis YA. J Appl Mech 1999;66(4):1026–8.
[17] Yarin AL, Koombhongse S, Reneker DH. J Appl Phys 2001;90: 4836–46.
[18] Gibson P, Rivin D, Kendrick C, Schreuder-Gibson H. Text Res J 1999;69(5):311–7.
[19] Huang L, McMillan RA, Apkarian RP, Pourdeyhimi B, Conticello VP, Chaikof EL. Macromolecules 2000;33:2989–97.
[20] Graham K, Ouyang M, Raether T, Grafe T, McDonald B, Knauf P. Polymeric nanofibers in air filtration applications. Proceedings of the 15th annual technical conference of the American Filtration and Separations Society; April 9–12, 2002.
[21] Zussman E, Yarin AL, Weihs D. Exp Fluids 2002;33:315–20.
[22] Koombhongse S, Liu W, Reneker DH. J Polym Sci, Part B: Polym Phys 2001;39(21):2598–606.
[23] Iwata T, Furuhashi Y, Su F, Doi Y. RINKEN Rev 2001;42:15–18.
[24] Berrill SA, Heatley F, Collett JH, Attwood D, Booth C, Fairclough JPA, Ryan AJ, Viras K, Dutton AJ, Blundell RS. J Mater Chem 1999; 9:1059–63.
[25] Wang Z, An L, Jiang W, Jiang B, Wang X. J Polym Sci, Part B: Polym Phys 1999;37:2682–91.
[26] Chen HL, Li LJ, Ou-Yang WC, Hwang JC, Wong WY. Macromolecules 1997;30:1718–22.
[27] Floudas G, Hilliou L, Lellinger D, Alig I. Macromolecules 2000;33: 6466–72.